THE JOURNAL OF PHYSICAL CHEMISTRY B

Article

pubs.acs.org/JPCB

Photoinitiated Electron Transfer in Zinc Porphyrin–Perylenediimide Cruciforms and Their Self-Assembled Oligomers

Sarah M. Mickley Conron, Leah E. Shoer, Amanda L. Smeigh, Annie Butler Ricks, and Michael R. Wasielewski*

Department of Chemistry and Argonne—Northwestern Solar Energy Research (ANSER) Center, Northwestern University, Evanston, Illinois 60208-3113, United States

Supporting Information

ABSTRACT: Two X-shaped, cruciform electron donor$_2$–acceptor–acceptor′$_2$ (D$_2$-A-A′$_2$) molecules, **1** and **2**, in which D = zinc 5-phenyl-10,15,20-tripentylporphyrin (ZnTPnP) or zinc 5,10,15,20-tetraphenylporphyrin (ZnTPP), respectively, A = pyromellitimide (PI), and A′ = perylene-3,4:9,10-bis-(dicarboximide) (PDI), were prepared to study self-assembly motifs that promote photoinitiated charge separation followed by electron and hole transport through π-stacked donors and acceptors. PDI secondary electron acceptors were chosen because of their propensity to form self-ordered, π-stacked assemblies in solution, while the ZnTPnP and ZnTPP donors were selected to test the effect of peripheral substituent steric interactions on the π-stacking characteristics of the cruciforms. Small- and wide-angle X-ray scattering measurements in toluene solution reveal that **1** assembles into a π-stacked structure having an average of 5 ± 1 molecules, when [**1**] ≅ 10^{-5} M, while **2** remains monomeric. Photoexcitation of the π-stacked structure of **1** results in formation of ZnTPnP$^{\bullet+}$-PI-PDI$^{\bullet-}$ in τ_{CS1} = 0.3 ps, which is nearly 100-fold faster than the formation of ZnTPnP$^{\bullet+}$-PI$^{\bullet-}$ in a model system lacking the PDI acceptor. The data are consistent with a self-assembled structure for **1** in which the majority of the intermolecular interactions have the ZnTPnP donor of one monomer cofacially π-stacked with the PDI acceptor of a neighboring monomer in a crisscrossed fashion. In contrast, **2** remains monomeric in toluene, so that photoexcitation of ZnTPP results in the charge separation reaction sequence: ^{1}*ZnTPP-PI-PDI → ZnTPP$^{\bullet+}$-PI$^{\bullet-}$-PDI → ZnTPP$^{\bullet+}$-PI-PDI$^{\bullet-}$, where τ_{CS1} = 33 ps and τ_{CS2} = 239 ps. The perpendicular orientation of ZnTPnP and ZnTPP relative to PDI in **1** and **2** is designed to decrease the porphyrin–PDI distance without greatly decreasing the overall number of bonds linking them. This serves to decrease the Coulomb energy penalty required to produce D$^{\bullet+}$-PI-PDI$^{\bullet-}$ relative to the corresponding linear D-PI-PDI array, while retaining the weak electronic coupling necessary to achieve long-lived charge separation, as evidenced by τ_{CR} = 24 ns for ZnTPP$^{\bullet+}$-PI-PDI$^{\bullet-}$.

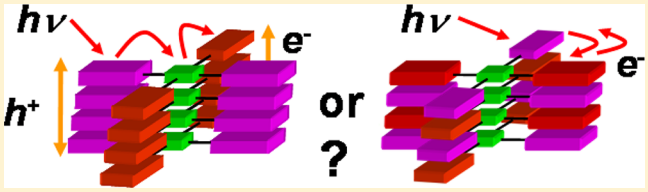

INTRODUCTION

Complex molecular assemblies of covalently bound electron donors and acceptors have been prepared to mimic both the light-harvesting and charge-separation functions of photosynthetic reaction center proteins.[1−7] Photoinitiated multistep electron transfer within these systems has been shown to rapidly separate charge with high quantum yields and store solar energy in the form of long-lived radical ion pairs (RPs, electron–hole pairs). Covalent systems having highly restricted molecular geometries and donor–acceptor distances allow for control over the initial light-harvesting and electron-transfer events, yet demand complex, multistep syntheses. We are currently developing an approach to photoactive materials for organic photovoltaics (OPVs) and artificial photosynthetic systems in which covalent building blocks are used to optimize the initial light-harvesting and charge-separation events, while self-assembly of these building blocks into large, ordered, supramolecular arrays is used to construct long pathways over which efficient charge transport can occur. Increasing molecular order within photoactive OPV materials correlates well with improved charge mobilities and OPV performance.[8] The use of self-assembly allows for increased order while retaining the ease of processing that is the hallmark of OPV materials. A conceptual model of a self-ordering functional organic material having efficient photodriven charge separation and subsequent transport of holes and electrons to the electrodes in an OPV is depicted in Figure 1. In this model, efficient photoinitiated multistep charge separation occurs within a covalently linked donor–acceptor building block, resulting in formation of a long-lived RP in which the charges are only very weakly bound by their Coulombic attraction. Self-assembly of these covalent donor–acceptor building blocks into a structure with segregated stacks of donors and acceptors allows the oxidized donor and the reduced acceptor to electronically interact with their corresponding neutral π-stacked neighbors with sufficient strength to overcome the weak Coulombic barrier between the charges in the covalent building block. Efficient transport of the separated charges within the π-stacked, segregated donor, and

Received: November 8, 2012
Revised: January 19, 2013
Published: January 29, 2013

   dx.doi.org/10.1021/jp311067q | J. Phys. Chem. B 2013, 117, 2195−2204

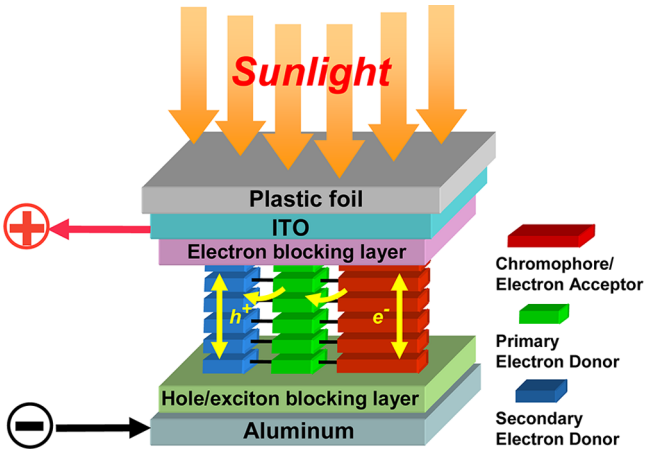

Figure 1. A multilayer organic solar cell in which covalent donor–acceptor building blocks are self-assembled to facilitate charge migration to the electrodes.

acceptor charge conduits to the OPV electrodes over the ~100–300 molecular layers needed absorb >90% of the incident photons requires that hopping of the weakly interacting, uncorrelated charges within the conduits is kinetically competitive with RP charge recombination.

Perylene-3,4:9,10-bis(dicarboximide) (PDI) and its derivatives have attracted a great deal of interest as visible chromophores for studies of energy and charge transport,[9−29] especially with regard to their potential applications as photoactive electron acceptors in organic photovoltaics.[30−44] Not only are PDIs thermally and photochemically stable,[45] they also exhibit a strong propensity to self-organize into ordered assemblies both in solution and in the solid phase by $\pi-\pi$ stacking interactions, often aided by hydrogen bonding and nano- and microsegregation.[9,11−29,46−53] For example, in one specific system having a zinc 5,10,15,20-tetraphenylporphyrin (ZnTPP) core covalently bound to four PDIs, ZnTPP-PDI_4, self-assembly in toluene produces nearly monodisperse cofacial pentameric assemblies in which are ZnTPP electron donors and PDI electron acceptors form segregated π-stacks.[21] Photogeneration of $ZnTPP^{\bullet+}$-$PDI^{\bullet-}$ occurs in τ = 12 ps for the pentamer and in τ = 20 ps for the monomeric reference molecule, while the corresponding charge recombination in the pentamer (τ_{CR} = 4.8 ns) is slightly longer than in the monomer (τ_{CR} = 3.0 ns).[21] While charge hopping through the π-stacked ZnTPP and PDI charge conduits may be competitive with the 4.8 ns $ZnTPP^{\bullet+}$-$PDI^{\bullet-}$ lifetime, it is unclear whether this lifetime is sufficiently long to permit efficient charge collection by an electrode that may be as many as 300 molecular layers away.

Further work aimed at photogenerating long-lived holes and electrons that migrate independently within two π-stacked charge conduits resulted in the synthesis of a symmetrically substituted PDI, in which two donor groups, aminopyrene (Apy) and *p*-diaminobenzene (DAB), are coupled to the chromophoric PDI acceptor through its imide positions, producing a linear $donor_2$–$donor_1$–acceptor–$donor_1$–$donor_2$ (D_2-D_1-A-D_1-D_2) system. This DAB-Apy-PDI-Apy-DAB system self-assembles via PDI π-stacking into a helical hexameric assembly in methylcyclohexane solution, which, upon photoexcitation, forms a long-lived ion pair state, $DAB^{\bullet+}$-Apy–$PDI^{\bullet-}$-Apy-DAB, in which the electrons migrate rapidly through the π-stacked PDIs.[24] The helical aggregate structure allows for π-stacking of the core PDI acceptors, but prevents the donors from π-stacking, so that the $DAB^{\bullet+}$ cation is trapped on a single molecule.

In the study described here, we synthesized two D-A-A′ cruciform molecules **1** and **2** in which D = zinc 5-phenyl-10,15,20-tripentylporphyrin or zinc 5,10,15,20-tetraphenylporphyrin, respectively, A = pyromellitimide (PI), and A′ = PDI. These structures were developed with two goals in mind: first, to examine the influence of donor and acceptor placement on the ability of these covalent building blocks to self-assemble into π-stacked donor–acceptor charge conduits; and second, to demonstrate an "around the corner" electron-transfer process using A as both the core linker and an active redox agent. As mentioned above, in most cases previously examined, PDIs show a strong propensity to self-associate, so that it is not known whether having an equal number of large, electron-rich, macrocyclic donors in the covalent D–A system will result in competitive donor–PDI self-association. Two likely π-stacking motifs for molecules **1** and **2** are illustrated in Figure 2, which

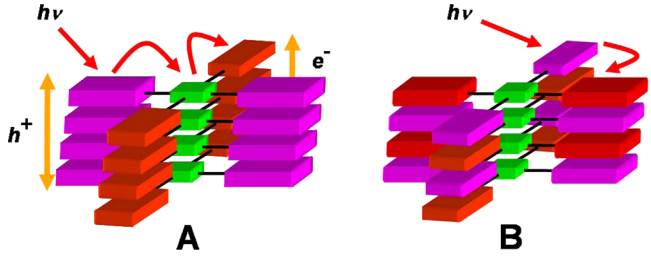

Figure 2. Schematic representation of possible π-stacking motifs formed by molecules **1** and **2**. Porphyrins are purple, PDIs are red, and PIs are green.

schematically shows the zinc porphyrin donor (purple), the primary pyromellitimide (PI) acceptor (green), and the PDI secondary acceptor (red). In structure A, the porphyrins and PDIs form segregated π-stacks, which can serve as noncovalent charge conduits for holes and electrons, respectively, while in structure B, ground-state charge-transfer interactions between the electron-rich porphyrins and the electron-deficient PDIs result in a crisscross arrangement of these molecules. Regarding the second point, the nature of the through-bond electron-transfer process within the cruciform monomers is such that the second electron-transfer step proceeds in a direction that is 90° to that of the first, which leads to a final $D^{\bullet+}$-A-$A'^{\bullet-}$ distance that is shorter than what would be found for a similar linear system. This facilitates the secondary charge separation step by decreasing the overall charge separation distance to minimize the Coulomb energy penalty required to separate the opposite charges, and at the same time retains the weak through-bond electronic coupling between the radical ions in the RP product necessary achieve slow charge recombination.

To aid the study of the electron-transfer mechanisms and supramolecular assembly of these cruciform systems, two model compounds lacking the PDI secondary electron acceptor were prepared. Compound **3** contains only the unsubstituted PI primary acceptor, while **4** has two naphthalene-1,8-dicarboximide (NMI) groups attached to the PI, which cannot be reduced by $PI^{\bullet-}$, but approximate the substituent effects of the PDIs attached to the PI. The self-assembly of **1** and **2** was studied using small- and wide-angle X-ray scattering in solution using a synchrotron source, while femtosecond and nanosecond

dx.doi.org/10.1021/jp311067q | J. Phys. Chem. B 2013, 117, 2195−2204

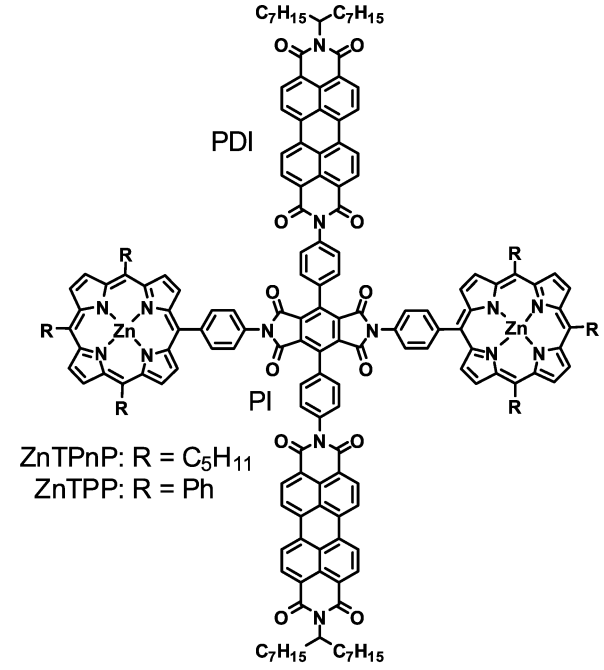

(ZnTPnP)$_2$-PI-(PDI)$_2$ (**1**)
(ZnTPP)$_2$-PI-(PDI)$_2$ (**2**)

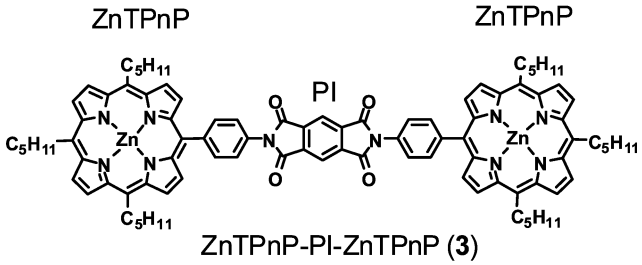

ZnTPnP-PI-ZnTPnP (**3**)

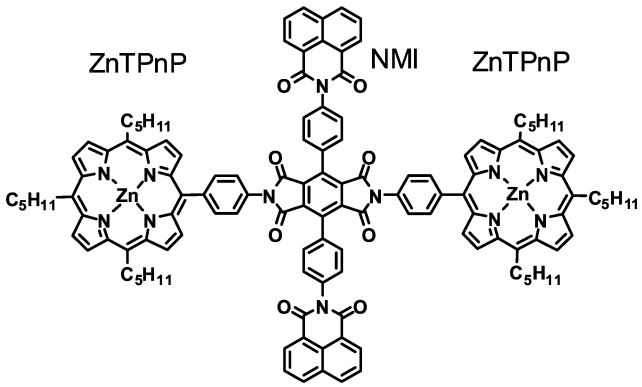

(ZnTPnP)$_2$-PI-(NMI)$_2$ (**4**)

transient absorption spectroscopy were used to characterize the electron-transfer processes within **1**−**4**.

EXPERIMENTAL METHODS

The synthesis and characterization of all final compounds and intermediates are described in detail in the Supporting Information. All reagents were purchased from Sigma-Aldrich and were used as received. All final products were purified by normal-phase preparative thin layer chromatography prior to characterization. Intermediates and final products were characterized by ^{1}H NMR, HRMS, and UV−vis spectroscopy.

X-ray Scattering. X-ray scattering measurements were performed using the undulator beamline at 12-ID at the Advanced Photon Source (APS) at Argonne National Laboratory. The X-ray scattering instrument utilized a double crystal Si(111) monochromator and a two-dimensional mosaic CCD detector.[54] The X-ray wavelength was set at λ = 0.62 Å and the sample to detector distance was adjusted to achieve scattering measured across the 0.007 Å^{-1} < q < 1.9 Å^{-1} region, where $q = (4\pi/\lambda) \sin\theta$, λ is the X-ray scattering wavelength and 2θ is the scattering angle. A quartz flow cell was used as the sample container. The concentrations of **1** and **2** in toluene were 1.1 × 10^{-5} and 7.0 × 10^{-6} M, respectively. All samples were filtered through 200 nm PTFE filters (Whatman) prior to measurements. The scattering intensity was averaged over 40 measurements and the solvent scattering was subtracted from the sample spectrum.

Optical Spectroscopy. All solvents used for optical spectroscopy were spectrophotometric grade and used as received, except for toluene, which was passed through a Glass Contour solvent purification system immediately prior to use. Ground-state absorption measurements were made on a Shimadzu UV-1800 spectrophotometer.

Femtosecond transient absorption (fsTA) measurements were made using the 130 fs, 416 nm frequency-doubled output from a 2 kHz regeneratively amplified Ti:sapphire laser system as the pump.[55] A white light continuum probe pulse was generated by focusing the IR fundamental into a 1 mm sapphire disk.[18] Detection with a CCD spectrograph has been described previously.[18] Samples of **1**−**4** were placed in a 2 mm path length glass cuvette and purged with nitrogen to prevent sample degradation. The concentrations of **1** and **2** were maintained at the same values used in the X-ray scattering experiments. The samples were irradiated with 1.0 μJ, 416 or 600 nm laser pulses focused to a 200 μm spot. Typically, 5−7 s of averaging was used to obtain the transient spectrum at a given delay time. The total instrument response function for the pump−probe experiments was 180 fs.

Samples for nanosecond transient absorption (nsTA) spectroscopy were placed in a 10 mm path length quartz cuvette equipped with a vacuum adapter and subjected to five freeze−pump-thaw degassing cycles. The nanosecond TA apparatus has been described previously;[24] however, the excitation laser used here is a Spectra-Physics Quanta Ray Lab 150 coupled to a Basiscan OPO (Spectra-Physics). The OPO output is directed to the sample and focused to slightly larger than the probe, ensuring efficient pump−probe overlap. An average of 100 sweeps per wavelength is collected at 5 nm intervals spanning 440−800 nm. Spectra are constructed from plotting specific time points of each kinetic with respect to the corresponding wavelength. The total instrument response time is 6 ns and is determined primarily by the laser pulse duration. Kinetic analyses were performed at several wavelengths using a Levenberg−Marquardt nonlinear least-squares fit to a sum of exponentials convoluted with a Gaussian instrument response function, while singular value decomposition of the 3D data set was carried out using Surface Xplorer 1.0 (Ultrafast Systems).[56]

RESULTS

Synthesis. The synthesis of compounds **1**−**4** is summarized in Schemes 1 and 2, and the details are given in the Supporting Information. Briefly, TPnP-NH$_2$[57] was condensed onto pyromellitimide (PI) in refluxing pyridine to produce TPnP-PI-TPnP (**5**). Subsequent metalation of the porphyrins using

dx.doi.org/10.1021/jp311067q | J. Phys. Chem. B 2013, 117, 2195−2204

Scheme 1. (a) Pyridine, $Zn(OAc)_2 \cdot 2H_2O$, Reflux, 28%; (b) $Zn(OAc)_2 \cdot 2H_2O$, 4:1 CH_2Cl_2:CH_3OH, Reflux, 87%; (c) Pyridine, $Zn(OAc)_2 \cdot 2H_2O$, Reflux, 53%; (d) 4:1 $CHCl_3$:CH_3OH, HCl, $SnCl_2 \cdot 2H_2O$, Reflux, 33%; (e) PIA, Pyridine, $Zn(OAc)_2 \cdot 2H_2O$, Reflux, 43%; (f) NMA, Pyridine, $Zn(OAc)_2 \cdot 2H_2O$, Reflux, 11%

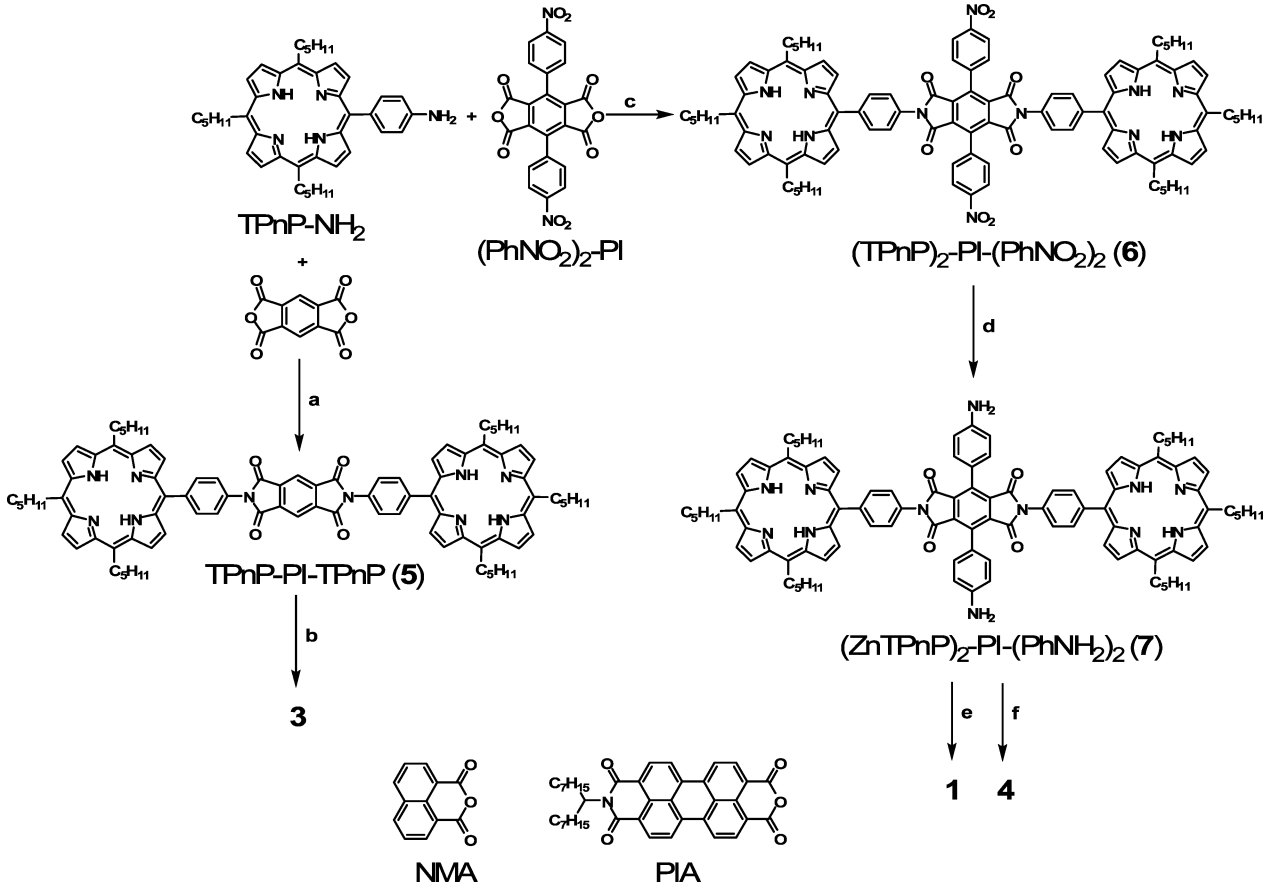

Scheme 2. Conditions: (a) HOAc, Reflux; (b) 2:1 $CHCl_3$:CH_3OH, HCl, $SnCl_2 \cdot 2H_2O$, Reflux, 39% over Two Steps; (c) PIA, Pyridine, $Zn(OAc)_2 \cdot 2H_2O$, Microwave, 200 °C, 30 min, 26%

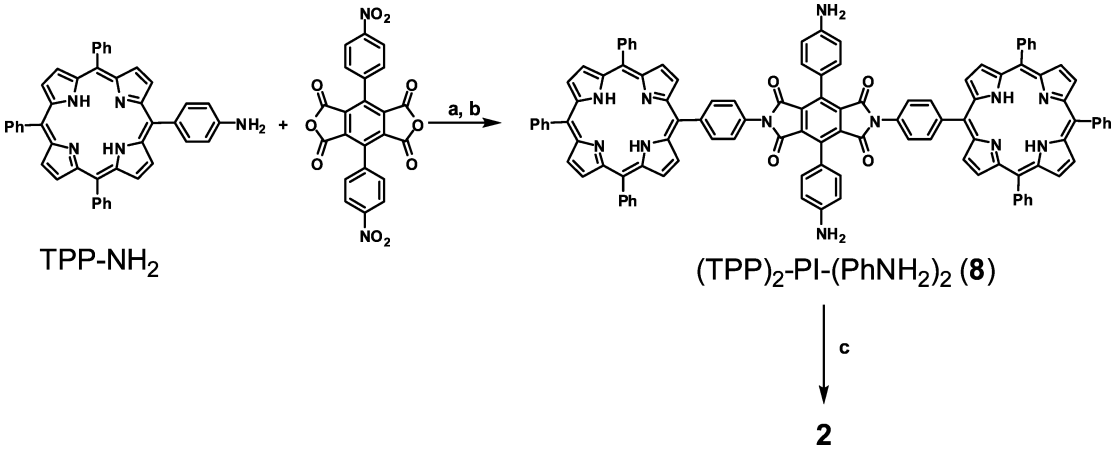

$Zn(OAc)_2$ yielded model compound **3** in quantitative yield. The syntheses of **1** and **4** were accomplished by first condensing TPnP-NH_2 onto PI-$(PhNO_2)_2$[12] in refluxing pyridine to produce $(TPnP)_2$-PI-$(PhNO_2)_2$ (**6**). The nitro groups in **6** were reduced to amines using $SnCl_2 \cdot 2H_2O$ and HCl, producing $(TPnP)_2$-PI-$(PhNH_2)_2$ (**7**) in 33% yield. From this intermediate, both **1** and **4** were synthesized via an imide condensation with PIA or NMA,[58] respectively. The synthetic route for **2**, shown in Scheme 2, follows a similar protocol. Condensation of 2 mol of TPP-NH_2[59] with PI-$(PhNO_2)_2$ produces $(TPP)_2$-PI-$(PhNO_2)_2$. Due to low solubility, the nitro groups of the crude product were reduced to amines using $SnCl_2 \cdot 2H_2O$ and HCl, producing $(TPP)_2$-PI-$(PhNH_2)_2$ (**8**). Condensation of **8** with 2 mol of PIA produced compound **2** in 26% yield.

Small- and Wide-Angle X-ray Scattering. Self-assembly of **1** and **2** in toluene was probed by small- and wide-angle X-ray scattering (SAXS/WAXS) experiments performed at the

dx.doi.org/10.1021/jp311067q | J. Phys. Chem. B 2013, 117, 2195−2204

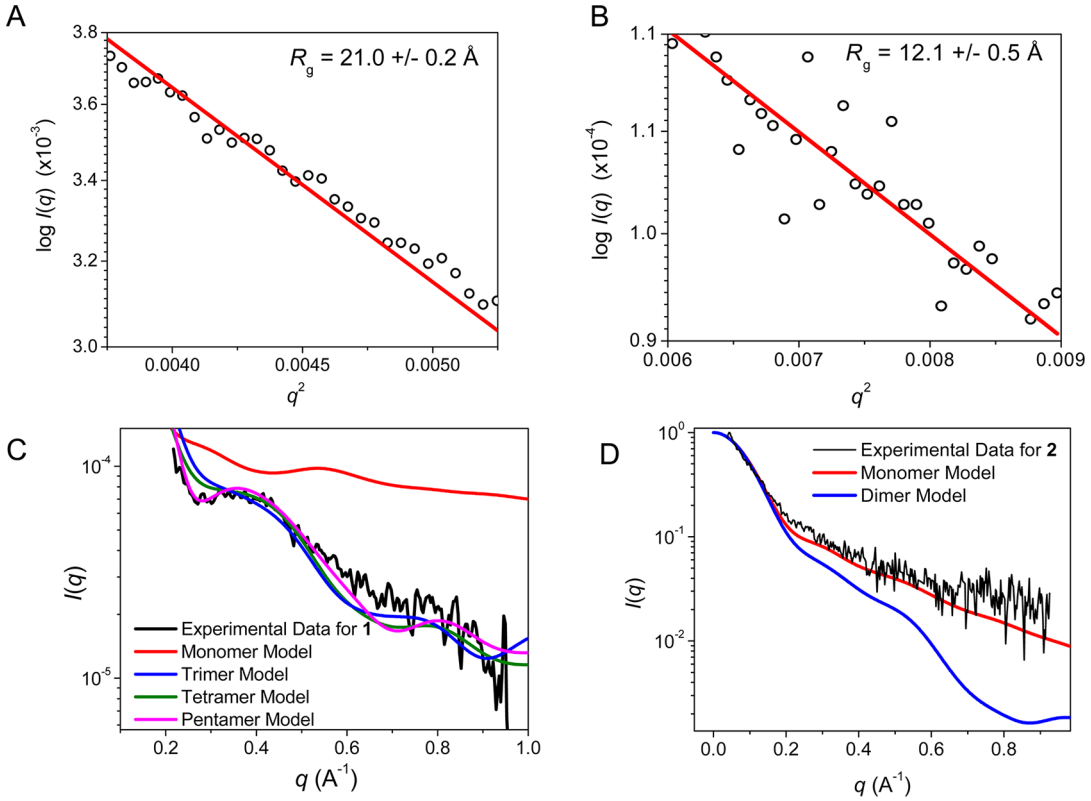

Figure 3. SAXS/WAXS data obtained in toluene. Guinier fits to the SAXS data for **1** (A) and **2** (B). Comparison of the scattering curves generated from the WAXS data with structural fits to the data for **1** (C) and **2** (D).

Advanced Photon Source at Argonne National Laboratory. In the low-resolution SAXS region, $q < 0.2$ Å^{-1}, the data were fit to the Guinier relationship

$$I(q) = I(0)\exp(-q^2R_g{}^2/3) \quad (1)$$

where $I(0)$ is the forward scattering amplitude and R_g is the radius of gyration of the assembly. Linear Guinier fits of the scattering data for **1** and **2** in the small-angle data regime are shown in Figure 3, A and B, respectively, which indicate the presence of molecular species well-approximated by spheres.[60] A least-squares fit to this region reveals that R_g = 21 Å for **1** and R_g = 12 Å for **2** in toluene. The radially averaged scattering intensities for **1** and **2** in the higher-resolution WAXS regime, $q > 0.2$ Å^{-1}, are shown in Figure 3, C and D, respectively. The experimental scattering curves were modeled by computing the scattering curves expected for the π-stacked geometries shown in Figures 2. Geometry-optimized π-stacked oligomers were generated using MM+ force field calculations.[61] No clear differentiation could be made between the segregated stacks (Figure 2A) and the crisscrossed stacks (Figure 2B).

Electron-Transfer Energetics. The ion pair energies of **1**−**4** were calculated using the Weller equation

$$\Delta G_{IP} = E_{ox} - E_{red} - \frac{e^2}{r_{DA}\varepsilon_s} + e^2\left(\frac{1}{2r_D} + \frac{1}{2r_A}\right)\left(\frac{1}{\varepsilon_s} - \frac{1}{\varepsilon_{sp}}\right) \quad (2)$$

where E_{ox} and E_{red} are the oxidation and reduction potentials of the donor and acceptor in a high polarity solvent having a dielectric constant of ε_{sp}, e is the charge of the electron, r_{DA} is the distance between donor and acceptor in the desired solvent with a dielectric constant of ε_s, and r_D and r_A are the ionic radii. The redox potentials used in the calculations are E_{ox} = 0.82 V for ZnTPP,[62] E_{ox} = 0.62 V for ZnTPnP,[57] E_{red} = −0.71 V for PI,[63] and E_{red} = −0.43 V for PDI (all vs SCE).[63] The ion pair distances, r_{DA}, were obtained from MM+ geometry-optimized structures[61] and are summarized in Table 1. For the ionic radii,

Table 1. Donor−Acceptor Distances and Resulting Ion Pair Energies for 1 and 2

molecule	r_{DA1} (Å)	E_{IP} (eV)
ZnTPnP$^{\bullet+}$-PI$^{\bullet-}$-PDI	12.5	1.76
ZnTPnP$^{\bullet+}$-PI-PDI$^{\bullet-}$	17.6	1.47
ZnTPP$^{\bullet+}$-PI$^{\bullet-}$-PDI	12.5	1.96
ZnTPP$^{\bullet+}$-PI-PDI$^{\bullet-}$	17.7	1.67

a value of r_D = 7 Å was used for ZnTPnP and ZnTPP, r_{A1} = 5 Å was used for PI, and r_{A2} = 7 Å was used for PDI.[62] The ion pair energies are summarized in Table 1, and Figure 4 depicts the possible energy and electron-transfer pathways, where ZnP = ZnTPnP or ZnTPP and ^{1}**ZnP E_{S2} = 2.92 eV, ^{1}*ZnP E_{S1} = 2.06 eV, ^{1}*PDI E_s = 2.25 eV, ^{3}*ZnP E_T = 1.7 eV,[64] and ^{3}*PDI E_T = 1.2 eV.[65]

Steady-State Spectroscopy. The ground-state absorption spectra for **1**−**4** are summarized in Figure 5. The spectra for model systems **3** and **4** are shown in toluene (Figure 5A) and are characterized by the intense ZnTPnP and ZnTPP B-band (Soret) absorption at 425 nm and the Q-band absorption features at about 556 and 597 nm. The absorption features of NMI in **4** are broad and overlap with the absorption features of PI at about 350 nm. The spectra of **1** in $CHCl_3$ and toluene are shown in Figure 5B. Earlier work has shown that chlorinated solvents such as $CHCl_3$ disaggregate PDI derivatives.[17] The

dx.doi.org/10.1021/jp311067q | J. Phys. Chem. B 2013, 117, 2195−2204

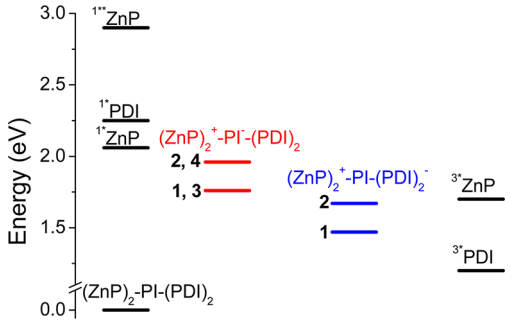

Figure 4. Energy levels of the relevant states in **1**−**4**, where ZnP = ZnTPnP or ZnTPP.

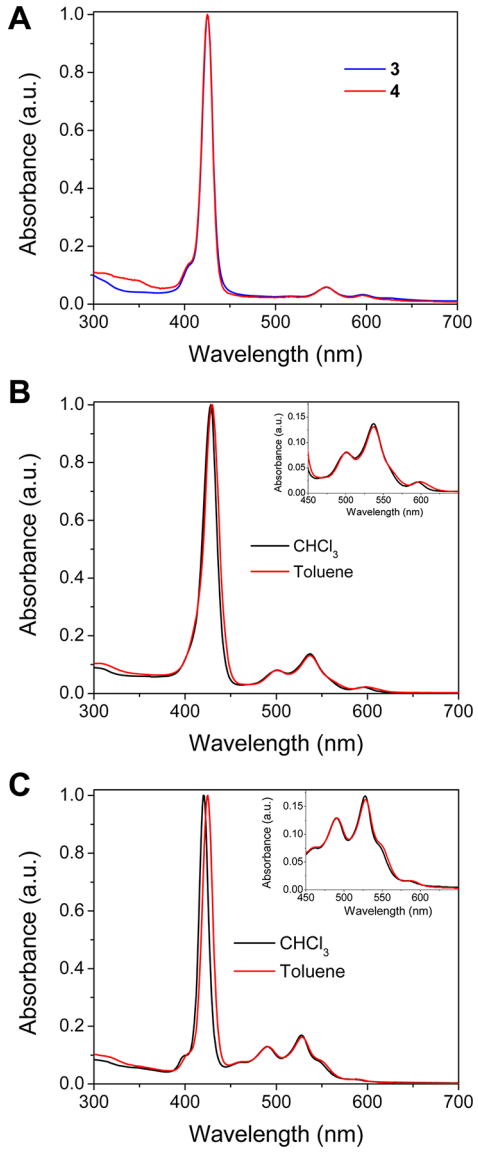

Figure 5. Ground-state absorption spectra of (A) model systems **3** and **4** in toluene, and (B) **1** and (C) **2** in the solvents listed, with insets showing an expansion of the 450−650 nm region.

spectra again show the characteristic Soret band at 425 nm. The characteristic (0,0) and (0,1) PDI absorption bands are observed at 540 and 500 nm, respectively, with the (0,0) absorption band displaying greater intensity than the (0,1) absorption band in both solvents. The absorption spectra for **2** in $CHCl_3$ and toluene are shown in Figure 5C. The spectra are similar to those of **1**. Insets within Figure 5, B and C, show an expanded view of the 450−645 nm spectral region.

Transient Absorption Spectroscopy. Molecules **1**−**4** were photoexcited with 416 nm, 130 fs laser pulses in toluene (Figure 6). Table 2 summarizes the relevant charge separation (τ_{CS1} and τ_{CS2}) and recombination (τ_{CR}) time constants obtained from the transient absorption kinetics.

Molecules **1** and **2** were also photoexcited at 600 nm in toluene, and the results of those experiments are also summarized in Table 2. The femtosecond transient absorption (fsTA) spectra of **1**−**4** with 416 nm photoexcitation in toluene are shown in Figure 6. The spectra of **3** show rapid formation of ^{1}*ZnTPnP at 460 nm (Figure 6A). The absorption features of ^{1}*ZnTPnP and ZnTPnP$^{\bullet+}$ are well-known to overlap in the region from 460 to 470 nm, with ZnTPnP$^{\bullet+}$ also weakly absorbing around 650 nm.[66−68] The characteristic absorption feature of PI$^{\bullet-}$ appears at 725 nm as a sharp peak in τ_{CS1} = 30 ps. The initial decay of the ^{1}*ZnTPnP feature to ZnTPnP$^{\bullet+}$ occurs simultaneously with the rise of the 725 nm PI$^{\bullet-}$ absorption feature. At longer times, the ion pair state ZnTPnP$^{\bullet+}$-PI$^{\bullet-}$ decays to form ^{3}*ZnTPnP-PI, with an absorption spectrum similar to that of ^{1}*ZnTPnP. The spectra of model compound **4** in toluene are similar to those of **3** (Figure 6B), with the PI$^{\bullet-}$ absorption feature in **4** appearing somewhat broader than in **3**.

The spectra of **1** in toluene at the earliest times show the appearance of the ^{1}*ZnTPnP/ZnTPnP$^{\bullet+}$ feature at 460 nm and a broad PDI$^{\bullet-}$ absorption feature from about 625 to 720 nm as well as PDI ground state bleaches at 500 and 540 nm and stimulated emission from ^{1}*ZnTPnP at 600 nm (Figure 6C). The fsTA spectra of **2** in toluene are again characterized by the ^{1}*ZnTPP/ZnTPP$^{\bullet+}$ absorption feature at 460 nm (Figure 6D). At early times, there is a broad PI$^{\bullet-}$ absorption feature at 720 nm that blue-shifts to 710 nm and becomes sharper as PDI$^{\bullet-}$ forms in τ_{CS2} = 239 ps. Because the ZnTPnP and ZnTPP Q-bands occur at 600 nm, and there is no PDI absorption at that wavelength, the Zn porphyrins in **1** and **2** in toluene were selectively photoexcited at 600 nm. The dynamics of charge separation and recombination with 600 nm photoexcitation are summarized in Table 2. The transient spectra were nearly identical to those of **1** and **2** obtained with 416 nm photoexcitation. Singular value decomposition (SVD) and global fitting of the 3-dimensional ΔA versus time and wavelength data sets of **1** and **2** resulted in decay-associated spectra and kinetic parameters (Figure S1 in the Supporting Information) consistent with those given in Figure 6 and Table 2.

The nanosecond transient absorption (nsTA) spectra of **2** in toluene are shown in Figure 7. The PDI$^{\bullet-}$ absorption feature at 710 nm decays with a lifetime of τ_{CR} = 23.5 ns. The residual absorption features at τ > 100 ns are attributed to formation of ^{3}*PDI.[65]

DISCUSSION

Characterization of Self-Assembled Structures. The SAXS/WAXS data for **1** and **2** were used to determine the size and shape of their respective solution-phase structures. Despite the small structural differences between monomeric **1** and **2**, the R_g values obtained from the Guinier fits to the SAXS data indicate that the solution-phase structure of **1** in toluene is almost twice as large as that of **2** (R_g = 21 and 12 Å,

dx.doi.org/10.1021/jp311067q | J. Phys. Chem. B 2013, 117, 2195−2204

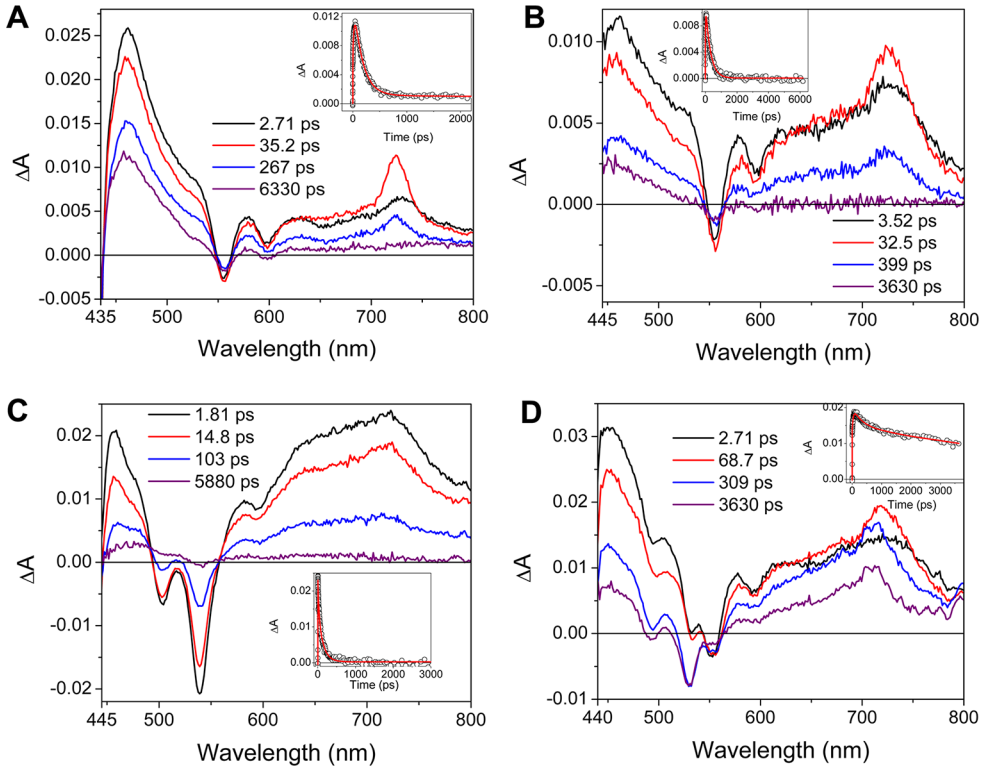

Figure 6. Femtosecond transient absorption spectra of (A) **3**, (B) **4**, (C) **1**, and (D) **2** in toluene following a 416 nm, 130 fs laser pulse. Insets: transient kinetics at 720 nm.

Table 2. Summary of Charge Separation (τ_{CS1} and τ_{CS2}) Recombination (τ_{CR}) Time Constants in 1-4 in Toluene Following Photoexcitation with 130 fs Laser Pulses

molecule	τ_{CS1} (ps)	τ_{CS2} (ps)	τ_{CR} (ps)
	532 nm Excitation		
1	0.3 ± 0.1	–	125 ± 17
2	33 ± 3	239 ± 27	24 ± 3 ns
3	30 ± 6	–	174 ± 11
4	26 ± 2	–	308 ± 21
	600 nm Excitation		
1	0.3 ± 0.1	–	84 ± 4
2	17 ± 1	239 ± 27	24 ± 3 ns

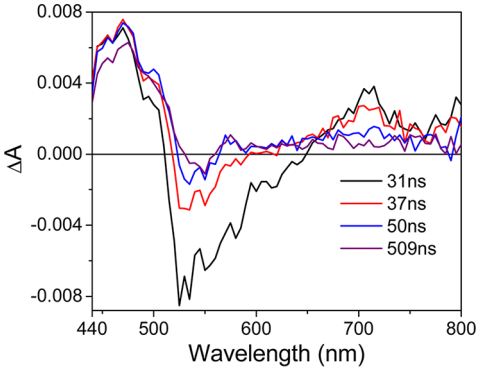

Figure 7. Nanosecond transient absorption spectra in toluene for **2** following a 6 ns, 416 nm laser pulse.

respectively). Modeling of the WAXS data in Figure 3C shows that the data cannot be fit by a simple monomer. The region of the scattering curve at q = 0.2–0.5 Å^{-1} is most sensitive to the size of the assembly. The best fit to the WAXS data shows that the assembly of **1** consists of 5 ± 1 molecules when the concentration of **1** in toluene is 1.1 × 10^{-5} M. Once again, it is important to note that the modeling cannot accurately tell the difference between segregated stacking (Figure 2A), criss-crossed stacking (Figure 2B), or a mixture thereof. In contrast, the WAXS data for **2** (Figure 3D) are readily modeled by a simple monomer. Even a dimer model deviates considerably from the experimental data. Thus, the SAXS/WAXS data suggest that the presence of the phenyl groups on ZnTPP provide significant steric hindrance to the formation of π-stacked assemblies, while the less sterically demanding *n*-pentyl groups allow significant aggregation of **1** at the concentrations used in these experiments. While the SAXS/WAXS data does not provide the evidence required to select between the π-stacking motifs shown in Figure 2, the UV–vis spectra of **1** in Figure 3 show that PDI does not π–π stack in the cofacial *H*-aggregate motif shown in Figure 2A. The UV–vis spectra of PDI for **1** in toluene have (0,0) and (0,1) absorption bands with nearly the same ratio in both $CHCl_3$, where **1** is monomeric, and in toluene, where the SAXS/WAXS data show that **1** is on average pentameric. It is well-known that exciton coupling of two PDI chromophores in an *H*-aggregate orientation results in an overall enhancement of the (0,1) vibronic band relative to the (0,0) band.[69] Thus, for the relatively small size of the assembly, the UV–vis data is consistent with a structure in which all of the monomers have the crisscrossed relationship between each other shown in Figure 2B.

Model Compound Electron-Transfer Dynamics. Model compounds **3** and **4** were studied to probe the dynamics of the initial electron transfer step from ^{1}*ZnTPnP to PI. In **4**, attachment of an electron-withdrawing NMI to the PI core via a

dx.doi.org/10.1021/jp311067q | J. Phys. Chem. B 2013, 117, 2195–2204

phenyl group mimics the electronic environment at PI in the cruciform systems, but because NMI has a very negative reduction potential (E_{red} = −1.37 V vs SCE),[63] it cannot be reduced by $PI^{\bullet-}$. The fsTA spectra of **3** and **4** in toluene are similar in appearance, and clearly show features at 710 nm characteristic of rapid formation of $PI^{\bullet-}$. The charge separation time constants in **3** and **4** are approximately the same (τ_{CS1} = ~30 ps), but the recombination time constant in **4** (τ_{CR} = 308 ps) is almost twice that of **3** (τ_{CR} = 174 ps). In both **3** and **4**, charge recombination takes place to form ^{3}*ZnTPnP, which is clear from the residual absorption features at 480 nm at τ > 3 ns.[64] Substitution of PI at its central benzene ring with an electron-withdrawing group makes PI slightly easier to reduce, which results in a more positive ΔG for charge recombination. Charge recombination yielding ^{3}*ZnTPnP is competitive with that giving the ZnTPnP ground state. The energy levels given in Figure 4 show that charge recombination to ^{3}*ZnTPnP is in the normal region of the Marcus rate versus free energy profile,[70] while charge recombination to ground state is in the inverted region. This is consistent with the total reorganization energy ($\lambda \cong 0.3-0.4$) for charge recombination of a closely related $ZnTPP^{\bullet+}$-$PI^{\bullet-}$ in toluene.[62] Thus, making ΔG_{CR} more positive should decrease the charge recombination rate to ^{3}*ZnTPnP and increase the rate of recombination to the ground state. The observed slowing of the charge recombination rate implies that charge recombination to the zinc porphyrin triplet dominates the overall charge recombination mechanism.

Electron-Transfer Dynamics in the Cruciforms. The fsTA spectra of **1** in toluene are very different from model compounds **3** and **4**. The ground-state bleach of PDI appears simultaneously with the ^{1}*ZnTPnP/$ZnTPnP^{\bullet+}$ absorption and the broad absorption at about 720 nm. The broad absorption at about 625−720 nm is similar to the absorption exhibited by π-stacked PDIs,[15,17] though the ground-state absorption spectrum of **1** in toluene does not exhibit the spectral characteristics typical of PDI *H*-aggregate formation. The charge separation and recombination time constants in **1** are shorter than those in **4**, which is surprising considering that in **4**, only the first electron-transfer step takes place, forming $ZnTPnP^{\bullet+}$-$PI^{\bullet-}$. However, the fact that the PDI ground-state bleach appears at the same time as the ^{1}*ZnTPnP/$ZnTPnP^{\bullet+}$ feature indicates that either ^{1}*PDI or $PDI^{\bullet-}$ is formed upon photoexcitation. Though there is a minimal PDI absorption at 416 nm that overlaps with the ZnTPnP Soret band, previous studies in our group on the photophysical properties of $ZnTPP-PDI_4$ revealed that ^{1}*PDI undergoes subpicosecond energy transfer to ZnTPP following preferential PDI photoexcitation at 545 nm.[21] Moreover, selective ZnTPnP photoexcitation at 600 nm results in identical behavior. This result implies that formation of $PDI^{\bullet-}$ in **1** is occurring by some pathway other than the intended intramolecular one, as formation of the initial ion pair state, $ZnTPnP^{\bullet+}$-$PI^{\bullet-}$-PDI, should take longer than the charge separation time constant observed for the π-stacked assembly of **1** in toluene. The charge recombination time constant for a linear ZnTPP-PDI system has been measured to be τ_{CR} = 3.0 ns.[21] If electron transfer is occurring from ^{1}*ZnTPnP to PDI via an intramolecular pathway that bypasses the bridging PI, the charge recombination time constant of $ZnTPnP^{\bullet+}$-PI-$PDI^{\bullet-}$ should be much longer than the measured τ_{CR} = 125 ps. In contrast, intermolecular electron transfer, between ZnTPnP in one molecule of **1** and a neighboring PDI in a second molecule of **1** to form ZnTPnP-PI-$PDI^{\bullet-}$/$ZnTPP^{\bullet+}$-PI-PDI, could explain the unexpectedly fast charge separation and recombination lifetimes in **1**. This process would likely result from π-stacking of a PDI from one monomer with a ZnTPnP of a second monomer, as depicted schematically in Figure 2B. Even though the $PDI^{\bullet-}$ absorption feature in **1** is very similar to that seen in cofacial assemblies of PDIs, it could very well result from the electronic effects of π-stacking of PDI with ZnTPP. Thus, both the transient absorption kinetics and the ground state UV−vis spectra of **1** are consistent with the crisscrossed structure for the assembly determined from the SAXS/WAXS data in toluene.

The electron-transfer process in **2** differs greatly from that of **1**. FsTA spectra of **2** in toluene (Figure 6D) show that the stepwise, intramolecular electron-transfer process takes place, with initial formation of $ZnTPP^{\bullet+}$-$PI^{\bullet-}$-PDI characterized by the $PI^{\bullet-}$ absorption feature at 720 nm in τ_{CS1} = 33 ps, similar to model compounds **3** and **4**. The second electron-transfer step to form $ZnTPP^{\bullet+}$-PI-$PDI^{\bullet-}$ occurs in τ_{CS2} = 239 ps and is characterized by a growth of the sharp absorption feature at 710 nm characteristic of monomeric $PDI^{\bullet-}$ and an increase in the intensity of the PDI ground-state bleach. The resulting ion pair state is long-lived, with charge recombination occurring in τ_{CR} = 24 ns. The residual absorption features in the nsTA spectra at τ > 100 ns are attributed to formation of ^{3}*ZnTPP-PI-PDI.

CONCLUSIONS

Small- and wide-angle X-ray scattering measurements in toluene solution reveal that **1** assembles into a π-stacked structure having an average of 5 ± 1 molecules, while **2** remains monomeric. The obvious differences in the electron-transfer pathways of **1** and **2** in toluene support the idea that the self-assembled structure of **1** is most likely the crisscrossed arrangement shown in Figure 2B, which short-circuits the formation of long-lived charge-separated species that can be readily formed in monomeric **2**. The electronic interaction of the electron-rich, sterically unencumbered ZnTPnP electron donors in cruciform structure **1** with the PDI electron acceptors in a neighboring molecule of **1** in the π-stacked assembly is stronger than the typical PDI−PDI interactions that drive formation of PDI-based nanostructures. Molecular designs that target segregated charge conduits for OPV applications will need to consider this issue.

ASSOCIATED CONTENT

Supporting Information

Experimental details including synthesis and characterization of **1**−**4**. This material is available free of charge via the Internet at http://pubs.acs.org.

AUTHOR INFORMATION

Corresponding Author

*E-mail: m-wasielewski@northwestern.edu.

Notes

The authors declare no competing financial interest.

ACKNOWLEDGMENTS

This work was supported by the Chemical Sciences, Geosciences, and Biosciences Division, Office of Basic Energy Sciences, DOE, under grant no. DE-FG02-99ER14999.

REFERENCES

(1) Wasielewski, M. R. Photoinduced Electron-Transfer in Supramolecular Systems for Artificial Photosynthesis. *Chem. Rev.* **1992**, *92*, 435−461.

(2) Gust, D.; Moore, T. A.; Moore, A. L. Mimicking Photosynthetic Solar Energy Transduction. *Acc. Chem. Res.* **2001**, *34*, 40−48.

(3) Holten, D.; Bocian, D. F.; Lindsey, J. S. Probing Electronic Communication in Covalently Linked Multiporphyrin Arrays. A Guide to the Rational Design of Molecular Photonic Devices. *Acc. Chem. Res.* **2002**, *35*, 57−69.

(4) Redmore, N. P.; Rubtsov, I. V.; Therien, M. J. Synthesis, Electronic Structure, and Electron Transfer Dynamics of (Aryl)-Ethynyl-Bridged Donor-Acceptor Systems. *J. Am. Chem. Soc.* **2003**, *125*, 8769−8778.

(5) Guldi, D. M. Biomimetic Assemblies of Carbon Nanostructures for Photochemical Energy Conversion. *J. Phys. Chem. B* **2005**, *109*, 11432−11441.

(6) Martin, N.; Sanchez, L.; Herranz, M. A.; Illescas, B.; Guldi, D. M. Electronic Communication in Tetrathiafulvalene (TTF)/C60 Systems: Toward Molecular Solar Energy Conversion Materials? *Acc. Chem. Res.* **2007**, *40*, 1015−1024.

(7) Moore, G. F.; Hambourger, M.; Gervaldo, M.; Poluektov, O. G.; Rajh, T.; Gust, D.; Moore, T. A.; Moore, A. L. A Bioinspired Construct That Mimics the Proton Coupled Electron Transfer between $P680^{\bullet+}$ and the Tyr_z-His190 Pair of Photosystem II. *J. Am. Chem. Soc.* **2008**, *130*, 10466−10467.

(8) Szarko, J. M.; Guo, J.-C.; Liang, Y.-Y.; Lee, B.-D.; Rolczynski, B. S.; Strzalka, J.; Xu, T.; Loser, S.; Marks, T. J.; Yu, L.-P.; Chen, L.-X. When Function Follows Form: Effects of Donor Copolymer Side Chains on Film Morphology and BHJ Solar Cell Performance. *Adv. Mater.* **2010**, *22*, 5468−5472.

(9) Würthner, F.; Thalacker, C.; Sautter, A. Hierarchical Organization of Functional Perylene Chromophores to Mesoscopic Superstructures by Hydrogen Bonding and π-π Interactions. *Adv. Mater.* **1999**, *11*, 754−758.

(10) Langhals, H.; Saulich, S. Bichromophoric Perylene Derivatives: Energy Transfer from Non-Fluorescent Chromophores. *Chem.—Eur. J.* **2002**, *8*, 5630−5643.

(11) Schenning, A.; Herrikhuyzen, J.; Jonkheijm, P.; Chen, Z.; Würthner, F.; Meijer, E. Photoinduced Electron Transfer in Hydrogen-Bonded Oligo(P-Phenylenevinylene)-Perylene Bisimide Chiral Assemblies. *J. Am. Chem. Soc.* **2002**, *124*, 10252−10253.

(12) Ahrens, M. J.; Sinks, L. E.; Rybtchinski, B.; Liu, W.; Jones, B. A.; Giaimo, J. M.; Gusev, A. V.; Goshe, A. J.; Tiede, D. M.; Wasielewski, M. R. Self-Assembly of Supramolecular Light-Harvesting Arrays from Covalent Multi-Chromophore Perylene-3,4:9,10-bis(dicarboximide) Building Blocks. *J. Am. Chem. Soc.* **2004**, *126*, 8284−8294.

(13) Li, X. Y.; Sinks, L. E.; Rybtchinski, B.; Wasielewski, M. R. Ultrafast Aggregate-to-Aggregate Energy Transfer within Self-Assembled Light-Harvesting Columns of Zinc Phthalocyanine Tetrakis(Perylenediimide). *J. Am. Chem. Soc.* **2004**, *126*, 10810−10811.

(14) Zhang, J.; Hoeben, F. J. M.; Pouderoijen, M. J.; Schenning, A. P. H.; Meijer, E. W.; Schryver, F. C.; De Feyter, S. Hydrogen-Bonded Oligo(p-Phenylenevinylene) Functionalized with Perylene Bisimide: Self-Assembly and Energy Transfer. *Chem.—Eur. J.* **2006**, *12*, 9046−9055.

(15) Rybtchinski, B.; Sinks, L. E.; Wasielewski, M. R. Photoinduced Electron Transfer in Self-Assembled Dimers of Three-Fold Symmetric Donor-Acceptor Molecules Based on Perylene-3,4:9,10-Bis-(dicarboximide). *J. Phys. Chem. A* **2004**, *108*, 7497−7505.

(16) Rybtchinski, B.; Sinks, L. E.; Wasielewski, M. R. Combining Light-Harvesting and Charge Separation in a Self-Assembled Artificial Photosynthetic System Based on Perylenediimide Chromophores. *J. Am. Chem. Soc.* **2004**, *126*, 12268−12269.

(17) van der Boom, T.; Hayes, R. T.; Zhao, Y.; Bushard, P. J.; Weiss, E. A.; Wasielewski, M. R. Charge Transport in Photofunctional Nanoparticles Self-Assembled from Zinc 5,10,15,20-Tetrakis(Perylene-Diimide)Porphyrin Building Blocks. *J. Am. Chem. Soc.* **2002**, *124*, 9582−9590.

(18) Giaimo, J. M.; Gusev, A. V.; Wasielewski, M. R. Excited-State Symmetry Breaking in Cofacial and Linear Dimers of a Green Perylenediimide Chlorophyll Analogue Leading to Ultrafast Charge Separation. *J. Am. Chem. Soc.* **2002**, *124*, 8530−8531.

(19) You, C.-C.; Würthner, F. Porphyrin-Perylene Bisimide Dyads and Triads: Synthesis and Optical and Coordination Properties. *Org. Lett.* **2004**, *6*, 2401−2404.

(20) Wasielewski, M. R. Energy, Charge, and Spin Transport in Molecules and Self-Assembled Nanostructures Inspired by Photosynthesis. *J. Org. Chem.* **2006**, *71*, 5051−5066.

(21) Ahrens, M. J.; Kelley, R. F.; Dance, Z. E. X.; Wasielewski, M. R. Photoinduced Charge Separation in Self-Assembled Cofacial Pentamers of Zinc-5,10,15,20-Tetrakis(perylenediimide)Porphyrin. *Phys. Chem. Chem. Phys.* **2007**, *9*, 1469−1478.

(22) Kaiser, T. E.; Wang, H.; Stepanenko, V.; Würthner, F. Supramolecular Construction of Fluorescent *J*-Aggregates Based on Hydrogen-Bonded Perylene Dyes. *Angew. Chem., Int. Ed.* **2007**, *46*, 5541−5544.

(23) Bullock, J. E.; Kelley, R. F.; Wasielewski, M. R. Self-Assembled Nanostructures for Organic Photovoltaics. *PMSE Prepr.* **2007**, *96*, 805−806.

(24) Bullock, J. E.; Carmieli, R.; Mickley, S. M.; Vura-Weis, J.; Wasielewski, M. R. Photoinitiated Charge Transport through Π-Stacked Electron Conduits in Supramolecular Ordered Assemblies of Donor−Acceptor Triads. *J. Am. Chem. Soc.* **2009**, *131*, 11919−11929.

(25) Kaiser, T. E.; Scheblykin, I. G.; Thomsson, D.; Würthner, F. Temperature-Dependent Exciton Dynamics in *J*-Aggregates-When Disorder Plays a Role. *J. Phys. Chem. B* **2009**, *113*, 15836−15842.

(26) Marciniak, H.; Li, X.-Q.; Wurthner, F.; Lochbrunner, S. One-Dimensional Exciton Diffusion in Perylene Bisimide Aggregates. *J. Phys. Chem. A* **2011**, *115*, 648−654.

(27) Ambrosek, D.; Marciniak, H.; Lochbrunner, S.; Tatchen, J.; Li, X.-Q.; Würthner, F.; Kuehn, O. Photophysical and Quantum Chemical Study on a *J*-Aggregate Forming Perylene Bisimide Monomer. *Phys. Chem. Chem. Phys.* **2011**, *13*, 17649−17657.

(28) Würthner, F.; Kaiser, T. E.; Saha-Moeller, C. R. *J*-Aggregates: From Serendipitous Discovery to Supramolecular Engineering of Functional Dye Materials. *Angew. Chem., Int. Ed.* **2011**, *50*, 3376−3410.

(29) Gunderson, V. L.; Krieg, E.; Vagnini, M. T.; Iron, M. A.; Rybtchinski, B.; Wasielewski, M. R. Photoinduced Singlet Charge Transfer in a Ruthenium(II) Perylene-3,4:9,10-Bis(Dicarboximide) Complex. *J. Phys. Chem. B* **2011**, *115*, 7533−7540.

(30) Tang, C. W. Two-Layer Organic Photovoltaic Cell. *App. Phys. Lett.* **1986**, *48*, 183−185.

(31) Ferrere, S.; Zaban, A.; Gregg, B. A. Dye Sensitization of Nanocrystalline Tin Oxide by Perylene Derivatives. *J. Phys. Chem. B* **1997**, *101*, 4490−4493.

(32) Dittmer, J. J.; Marseglia, E. A.; Friend, R. H. Electron Trapping in Dye/Polymer Blend Photovoltaic Cells. *Adv. Mater.* **2000**, *12*, 1270−1274.

(33) Gregg, B. A.; Cormier, R. A. Doping Molecular Semiconductors: n-Type Doping of a Liquid Crystal Perylene Diimide. *J. Am. Chem. Soc.* **2001**, *123*, 7959−7960.

(34) Schmidt-Mende, L.; Fechtenkotter, A.; Müllen, K.; Moons, E.; Friend, R. H.; MacKenzie, J. D. Self-Organized Discotic Liquid Crystals for High-Efficiency Organic Photovoltaics. *Science* **2001**, *293*, 1119−1122.

(35) Neuteboom, E. E.; Meskers, S. C. J.; van Hal, P. A.; van Duren, J. K. J.; Meijer, E. W.; Janssen, R. A. J.; Dupin, H.; Pourtois, G.; Cornil, J.; Lazzaroni, R.; Bredas, J. L.; Beljonne, D. Alternating Oligo(p-Phenylenevinylene)-Perylene Bisimide Copolymers: Synthesis, Photophysics, and Photovoltaic Properties of a New Class of Donor-Acceptor Materials. *J. Am. Chem. Soc.* **2003**, *125*, 8625−8638.

(36) Shin, W. S.; Jeong, H.-H.; Kim, M.-K.; Jin, S.-H.; Kim, M.-R.; Lee, J.-K.; Lee, J. W.; Gal, Y.-S. Effects of Functional Groups at

Perylene Diimide Derivatives on Organic Photovoltaic Device Application. *J. Mater. Chem.* **2006**, *16*, 384−390.
(37) Kim, M. H.; Cho, M. J.; Kim, K. H.; Hoang, M. H.; Lee, T. W.; Jin, J.-I.; Kang, N. S.; Yu, J.-W.; Choi, D. H. Organic Donor-Σ-Acceptor Molecules Based on 1,2,4,5-Tetrakis((E)-2-(5′-Hexyl-2,2′-Bithiophen-5-Yl)Vinyl)Benzene and Perylene Diimide Derivative and Their Application to Photovoltaic Devices. *Org. Electron.* **2009**, *10*, 1429−1441.
(38) Woodhouse, M.; Perkins, C. L.; Rawls, M. T.; Cormier, R. A.; Liang, Z.; Nardes, A. M.; Gregg, B. A. Non-Conjugated Polymers for Organic Photovoltaics: Physical and Optoelectronic Properties of Poly(Perylene Diimides). *J. Phys. Chem. C* **2010**, *114*, 6784−6790.
(39) Hains, A. W.; Chen, H.-Y.; Reilly, T. H., III; Gregg, B. A. Cross-Linked Perylene Diimide-Based N-Type Interfacial Layer for Inverted Organic Photovoltaic Devices. *ACS Appl. Mater. Interfaces* **2011**, *3*, 4381−4387.
(40) Zhan, X.; Facchetti, A.; Barlow, S.; Marks, T. J.; Ratner, M. A.; Wasielewski, M. R.; Marder, S. R. Rylene and Related Diimides for Organic Electronics. *Adv. Mater.* **2011**, *23*, 268−284.
(41) Liang, Z.; Cormier, R. A.; Nardes, A. M.; Gregg, B. A. Developing Perylene Diimide Based Acceptor Polymers for Organic Photovoltaics. *Synth. Met.* **2011**, *161*, 1014−1021.
(42) Keivanidis, P. E.; Kamm, V.; Zhang, W.; Floudas, G.; Laquai, F.; McCulloch, I.; Bradley, D. D. C.; Nelson, J. Correlating Emissive Non-Geminate Charge Recombination with Photocurrent Generation Efficiency in Polymer/Perylene Diimide Organic Photovoltaic Blend Films. *Adv. Funct. Mater.* **2012**, *22*, 2318−2326.
(43) Raj, M. R.; Anandan, S.; Solomon, R. V.; Venuvanalingam, P.; Iyer, S. S. K.; Ashokkumar, M. Synthesis of Conjugated Perylene Diimide-Based Copolymer with 5,5′-Bis(4-Aminophenyl)-2−2′-Bifuryl Moiety as an Active Material for Organic Photovoltaics. *J. Photochem. Photobiol., A* **2012**, *247*, 52−62.
(44) Rajaram, S.; Shivanna, R.; Kandappa, S. K.; Narayan, K. S. Nonplanar Perylene Diimides as Potential Alternatives to Fullerenes in Organic Solar Cells. *J. Phys. Chem. Lett.* **2012**, *3*, 2405−2408.
(45) Langhals, H.; Ismael, R. Cyclophanes as Model Compounds for Permanent, Dynamic Aggregates. Induced Chirality with Strong CD Effects. *Eur. J. Org. Chem.* **1998**, 1915−1917.
(46) Thalacker, C.; Würthner, F. Chiral Perylene Bisimide-Melamine Assemblies: Hydrogen Bond-Directed Growth of Helically Stacked Dyes with Chiroptical Properties. *Adv. Funct. Mater.* **2002**, *12*, 209−218.
(47) Wang, W.; Li, L. S.; Helms, G.; Zhou, H. H.; Li, A. D. Q. To Fold or to Assemble? *J. Am. Chem. Soc.* **2003**, *125*, 1120−1121.
(48) Würthner, F. Perylene Bisimide Dyes as Versatile Building Blocks for Functional Supramolecular Architectures. *Chem. Commun.* **2004**, 1564−1579.
(49) Yan, P.; Chowdhury, A.; Holman, M. W.; Adams, D. M. Self-Organized Perylene Diimide Nanofibers. *J. Phys. Chem. B* **2005**, *109*, 724−730.
(50) Chen, Z.; Baumeister, U.; Tschierske, C.; Würthner, F. Effect of Core Twisting on Self-Assembly and Optical Properties of Perylene Bisimide Dyes in Solution and Columnar Liquid Crystalline Phases. *Chem.—Eur. J.* **2007**, *13*, 450−465.
(51) Ghosh, S.; Li, X.-Q.; Stepanenko, V.; Würthner, F. Control of H- and J-Type Π Stacking by Peripheral Alkyl Chains and Self-Sorting Phenomena in Perylene Bisimide Homo- and Heteroaggregates. *Chem.—Eur. J.* **2008**, *14*, 11343−11357.
(52) Dehm, V.; Buechner, M.; Seibt, J.; Engel, V.; Würthner, F. Foldamer with a Spiral Perylene Bisimide Staircase Aggregate Structure. *Chem. Sci.* **2011**, *2*, 2094−2100.
(53) Xie, Z.; Stepanenko, V.; Radacki, K.; Würthner, F. Chiral J-Aggregates of Atropo-Enantiomeric Perylene Bisimides and Their Self-Sorting Behavior. *Chem.—Eur. J.* **2012**, *18*, 7060−7070.
(54) Seifert, S.; Winans, R. E.; Tiede, D. M.; Thiyagarajan, P. Design and Performance of a Asaxs (Anomalous Small Angle X-Ray Scattering) Instrument at the Advanced Photon Source. *J. Appl. Crystallogr.* **2000**, *33*, 782−784.
(55) Weiss, E. A.; Ahrens, M. J.; Sinks, L. E.; Gusev, A. V.; Ratner, M. A.; Wasielewski, M. R. Making a Molecular Wire: Charge and Spin Transport through Para-Phenylene Oligomers. *J. Am. Chem. Soc.* **2004**, *126*, 5577−5584.
(56) *Surface Xplorer*; Ultrafast Systems LLC: Sarasota, FL 34234.
(57) Kelley, R. F.; Shin, W. S.; Rybtchinski, B.; Sinks, L. E.; Wasielewski, M. R. Photoinitiated Charge Transport in Supramolecular Assemblies of a 1,7,N,N′-Tetrakis(Zinc Porphyrin)-Perylene-3,4:9,10-Bis(dicarboximide). *J. Am. Chem. Soc.* **2007**, *129*, 3173−3181.
(58) Holman, M. W.; Liu, R. C.; Adams, D. M. Single-Molecule Spectroscopy of Interfacial Electron Transfer. *J. Am. Chem. Soc.* **2003**, *125*, 12649−12654.
(59) Brousmiche, D. W.; Serin, J. M.; Frechet, J. M. J.; He, G. S.; Lin, T.-C.; Chung, S. J.; Prasad, P. N. Fluorescence Resonance Energy Transfer in a Novel Two-Photon Absorbing System. *J. Am. Chem. Soc.* **2003**, *125*, 1448−1449.
(60) Svergun, D. I.; Koch, M. H. Small-Angle Scattering Studies of Biological Macromolecules in Solution. *Rep. Prog. Phys.* **2003**, *66*, 1735−1782.
(61) Hypercube Inc.: 1115 NW 4th Street, Florida 32601, 1994.
(62) Hayes, R. T.; Walsh, C. J.; Wasielewski, M. R. Competitive Electron Transfer from the S_2 and S_1 Excited States of Zinc Meso-Tetraphenylporphyrin to a Covalently Bound Pyromellitimide: Dependence on Donor-Acceptor Structure and Solvent. *J. Phys. Chem. A* **2004**, *108*, 2375−2381.
(63) Gosztola, D.; Niemczyk, M. P.; Svec, W.; Lukas, A. S.; Wasielewski, M. R. Excited Doublet States of Electrochemically Generated Aromatic Imide and Diimide Radical Anions. *J. Phys. Chem. A* **2000**, *104*, 6545−6551.
(64) Leenstra, W. R.; Gouterman, M.; Kwiram, A. L. Nonradiative Character of the Triplet Sublevels in Zinc Tetraphenylporphyrin. *Chem. Phys. Lett.* **1979**, *65*, 278−280.
(65) Ford, W. E.; Kamat, P. V. Photochemistry of 3,4,9,10-Perylenetetracarboxylic Dianhydride Dyes. 3. Singlet and Triplet Excited-State Properties of the Bis(2,5-di-tert-Butyl Phenyl)Imide Derivative. *J. Phys. Chem.* **1987**, *91*, 6373−6380.
(66) Imahori, H.; Yamada, K.; Hasegawa, M.; Taniguchi, S.; Okada, T.; Sakata, Y. A Sequential Photoinduced Electron Relay Accelerated by Fullerene in a Porphyrin-Pyromellitimide-C60 Triad. *Angew. Chem., Int. Ed. Engl.* **1997**, *36*, 2626−2629.
(67) Yamada, K.; Imahori, H.; Yoshizawa, E.; Gosztola, D.; Wasielewski, M. R.; Sakata, Y. Self-Assembly of Zincporphyrin Dimer and Pyromellitimide Using Two Coordination Bonds and Photoinduced Intramolecular Electron Transfer. *Chem. Lett.* **1999**, 235−236.
(68) Fajer, J.; Borg, D. C.; Forman, A.; Dolphin, D.; Felton, R. H. Pi-Cation Radicals and Dications of Metalloporphyrins. *J. Am. Chem. Soc.* **1970**, *92*, 3451−3459.
(69) Giaimo, J. M.; Lockard, J. V.; Sinks, L. E.; Scott, A. M.; Wilson, T. M.; Wasielewski, M. R. Excited Singlet States of Covalently Bound, Cofacial Dimers and Trimers of Perylene-3,4:9,10-Bis-(Dicarboximide)S. *J. Phys. Chem. A* **2008**, *112*, 2322−2330.
(70) Marcus, R. A. On Theory of Electron-Transfer Reactions. VI. Unified Treatment for Homogeneous and Electrode Reactions. *J. Chem. Phys.* **1965**, *43*, 679−701.